Electronic Supplementary Information (ESI)

Ultrahigh sensitivity upconversion low temperature sensors via manipulating the non-thermally coupled levels of Er^{3+} ions

Weitao Ying,[a] Jingyi He,[a] Xuemei Fan,[a] Shiqing Xu,*[a] Jianmin Gu*[a,b] and Shimin Liu*[a]

[a]State Key Laboratory of Metastable Materials Science and Technology (MMST), Yanshan University, Qinhuangdao 066004, China

[b]Hebei Key Laboratory of Applied Chemistry, School of Environmental and Chemical Engineering, Yanshan University, Qinhuangdao 066004, China

*Corresponding author. E-mail: ysuxsq@ysu.edu.cn; jmgu@ysu.edu.cn; lsm@ysu.edu.cn.

Experimental

***Materials*:** All of the chemical reagents used in this experiment are analytical grade and were received without additional treatment. The raw materials of SiO_2, Al_2O_3, Na_2CO_3, NaF, YF_3, ErF_3 and YbF_3 were all purchased from Aladdin Reagent.

Preparation:

The precursor glass (PG) sample was synthetized from the composition of $58SiO_2$-$6Al_2O_3$-$18Na_2CO_3$-12NaF-$5YF_3$-$1.5ErF_3$-1.5 YbF_3 (mol%) via the traditional melting-quenching method. The raw materials were weighed and ground, then put into a alumina crucible at 1500 °C for 30 minutes in air atmosphere. Subsequently, the melt was casted onto a 450 °C preheated stainless-steel plate to form PG. Finally, the transparent glass ceramic (GC) containing Er,Yb: NaYF4 nanocrystals was synthetized via thermal treating the PG at 600 °C for 2 h.

***Measurements*:**

D/MAX-2500PC X-ray diffractometer was utilized for XRD analysis. The transmission electron microscopy (TEM, JEM-2010) was used to study microstructure of GC sample. Furthermore, STEM operated in the high-angle annular dark-field (HAADF) mode was also performed. UC luminescence spectrs was obtainedthrough Fluorolog-3 fluorescence spectrometer with optical detection equipment, where 980 nm and 1550 nm lasers as excitation source. The temperature around the GC sample in the spectra test was controlled via the temperature control system TC 202, with a range of 90-300K.

Figure S1. Cryogenic control equipment. Cooperate with the fluorescence spectrometer to realize temperature-dependent spectra testing.

The UC emission spectra of GC sample at different temperatures are realized based on this device, where the temperature is controlled by liquid nitrogen and heaters. The measurement resolution is 0.01 K, and the temperature measurement error is less than 0.05% F.S.

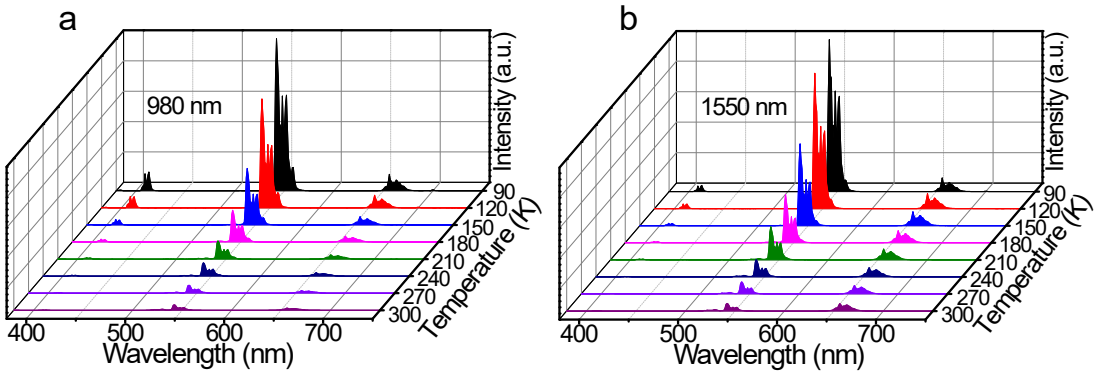

Figure S2. UC emission spectra of GC sample upon (a) 980 and (b) 1550 nm excitation at various temperatures from 90 K to 300 K.

The temperature-dependent UC spectra of GC sample upon (a) 980 nm and (b) 1550 nm laser excitation are shown in Figure S2, where the emission of the sample change as the temperature change. The four UC emission peaks observed are named B (409 nm), G1 (530 nm), G2 (542 nm) and R (656 nm), respectively. The B, G2 and R emission intensities decreased monotonously with the increasing temperature, while the G1 (530 nm) emission intensity increased under the condition of whether 980 nm or 1550 nm laser excitation.

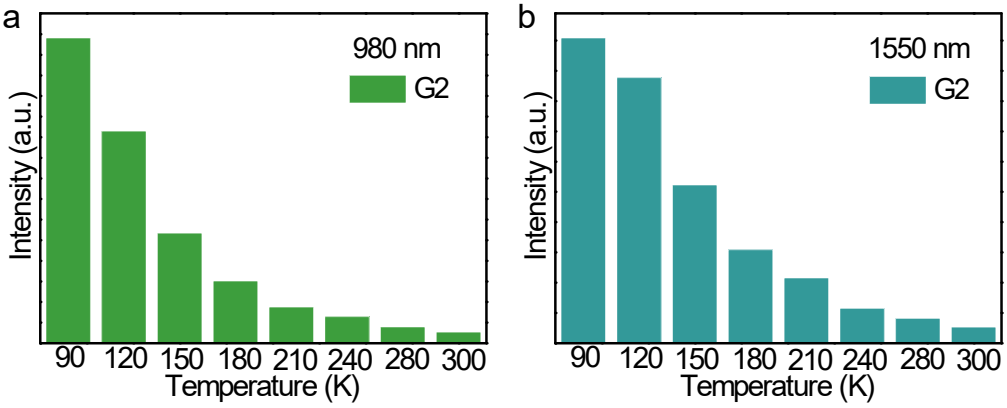

Figure S3. The integrated UC intensities of G2 emission at various temperatures under (a) 980 and (b) 1550 nm excitation.

Under whether 980 nm or 1550 nm laser excitation, the intensity of G2 emission decreases sharply with the increase of temperature, indicating that temperature has a great influence on the luminescence intensity of G2 emission.

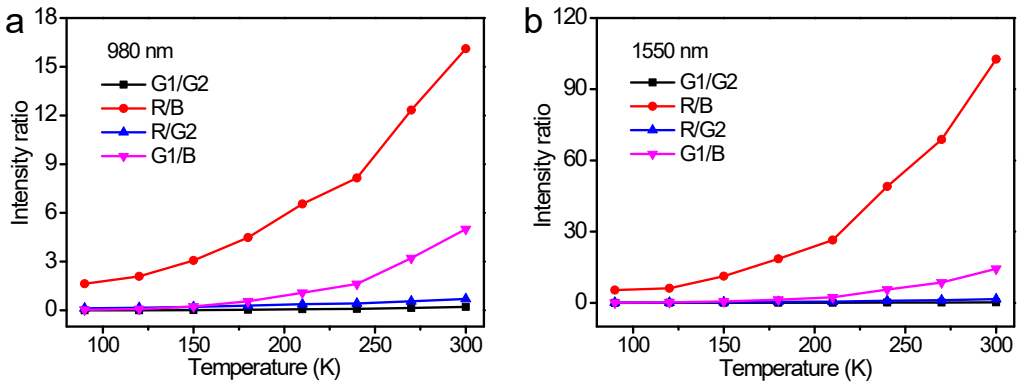

Figure S4. The emission ratios of G1/G2, R/B, R/G2 and G1/B at various temperatures under (a) 980 nm and (b) 1550 nm laser excitation.

Under 980 nm or 1550 nm excitation, the intensity ratios of G1/G2, R/B, R/G2 and G1/B are displayed in Figure S4, which can be observed that all the ratios keep enhancing with the increasing of temperature. It is worth noting that the ratios of R/B and G1/B change more obviously with temperature, which indicates that the non-thermal couple energy levels (NTCL) composed of red-blue emission levels and green-blue emission levels are more suitable for temperature sensing. The high emission intensity ratio could further ensure the high sensitivity based on optical temperature measurement of fluorescence intensity ratio (FIR) technique.

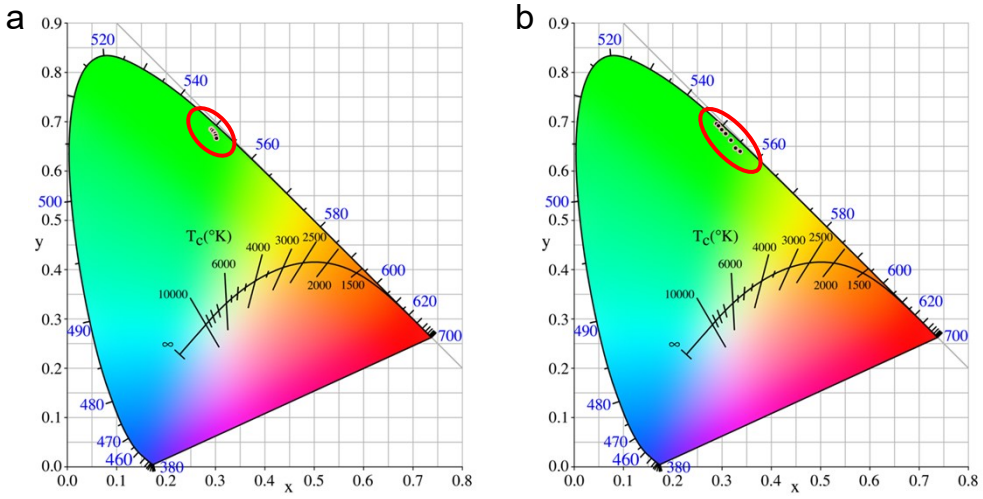

Figure S5. CIE chromaticity diagram showing chromaticity points of the GC material at various temperature. Under (a) 980 nm and (b) 1550 nm laser excitation.

It can be observed in Figure S7 that the color of the GC material is concentrated in the green area under 980 nm laser excitation, where the color coordinates gradually move to the yellow area as the temperature increases. Similarly, the color of the GC material also move to the yellow area with increasing temperature upon 1550 nm excitation, where the magnitude of the color coordinates shift is larger compared to the 980 nm excitation.

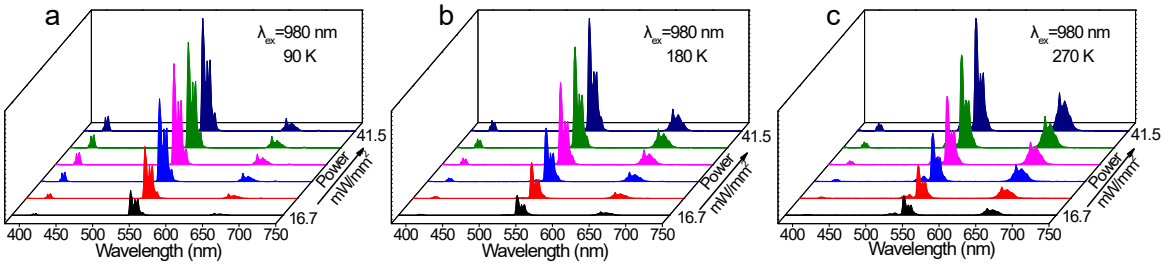

Figure S6. Dependences of UC spectra on excitation power under 980 nm laser. The UC emission spectra related to excitation power density at (a) 90 K, (b) 180 K, and (c) 270 K.

The UC emission spectra under different excitation power density of 980 nm laser are shown in Figure S6, which the UC emission intensity of the GC sample increase with the increase of power density. Through the dependence of UC spectra on the excitation power, we can get the number of photons that need to be absorbed to complete the blue, green and red emission under different temperature conditions according to the formula $I_{UC} \propto P^n$. In the formula, I_{UC} is the emission intensity, P is the power of the pump laser, and n is the number of photons.

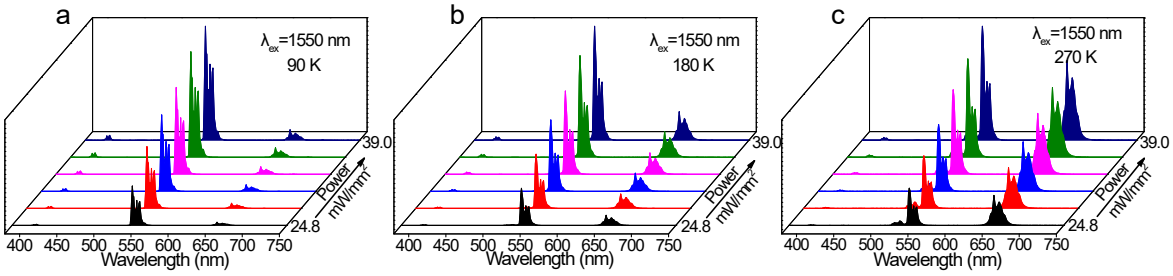

Figure S7. Dependences of UC spectra on excitation power under 1550 nm laser. The UC emission spectra related to excitation power density at (a) 90 K, (b) 180 K, and (c) 270 K.

The UC emission spectra under different excitation power density of 1550 nm laser are shown in Figure S7, which the intensity of all UC emission bands of the GC sample increase with the increase of power density. Similarly, we can get the number of photons that need to be absorbed to complete the blue, green and red emission under different temperature conditions according to the formula $I_{UC} \propto P^n$.

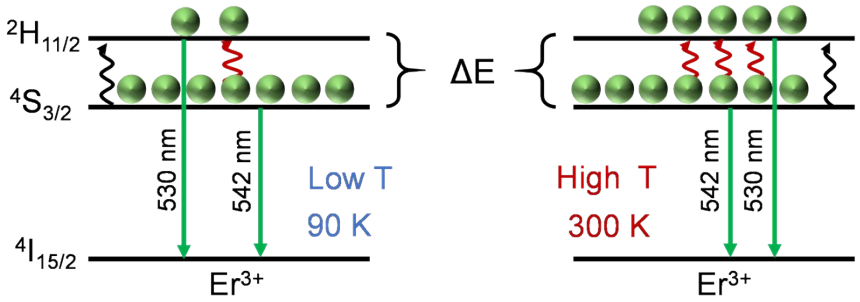

Figure S8. Proposed mechanism for green UC emissions assigned to the $^2H_{11/2}\rightarrow{}^4I_{15/2}$ and $^4S_{3/2}\rightarrow{}^4I_{15/2}$ transitions of Er^{3+}, showing the different population ratios for the $^2H_{11/2}$ and $^4S_{3/2}$ states of Er^{3+} under different temperature.

The population of the two green-emitting states of Er^{3+} ions ($^2H_{11/2}$ and $^4S_{3/2}$) present the characteristics of Boltzmann distribution. On account of the small energy gap between the $^2H_{11/2}$ and $^4S_{3/2}$ levels, this energy separation may allow the $^2H_{11/2}$ levels to be populated by thermal excitation from the excited $^4S_{3/2}$ levels. At low temperature, electrons of the $^2H_{11/2}$ levels is difficult be filled efficiently due to low thermal activation energy, resulting in weak emission of $^2H_{11/2}$ levels. With the increase of temperature, more electrons will transit from the $^4S_{3/2}$ levels to the $^2H_{11/2}$ levels through thermal excitation, which lead to the UC emission at the $^2H_{11/2}$ levels (530 nm) gradually enhanced.

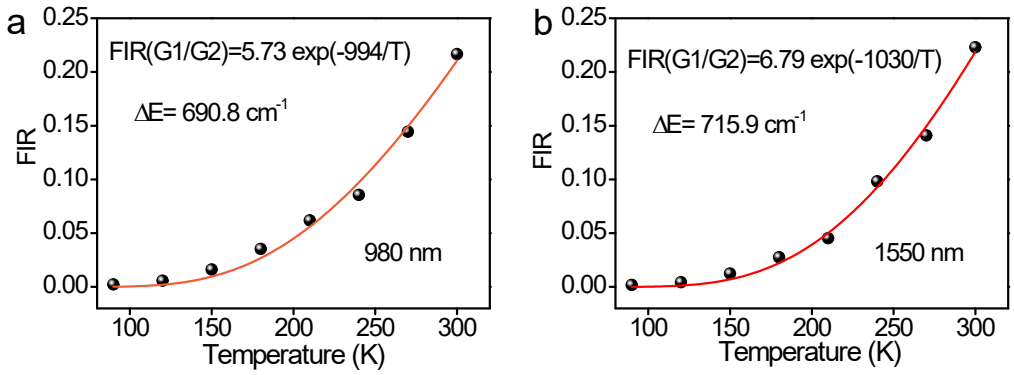

Figure S9. Temperature dependence of FIR based on TCL of $^2H_{11/2}/^4S_{3/2}$ under (a) 980 nm and (b) 1550 nm excitation.

With the increase of temperature, the luminescence intensity of 530 nm has increased, while the luminescence intensity of 542 nm has decreased significantly. The FIR based on thermal couple levels (TCL) enhances gradually with the increase of temperature. Under 980 nm and 1550 nm excitation, the corresponding relative population for the thermally coupled electronic states can be mathematically expressed as: FIR(G1/G2)=5.73exp(-994/T) and FIR(G1/G2)=6.79exp(-1030/T), respectively.

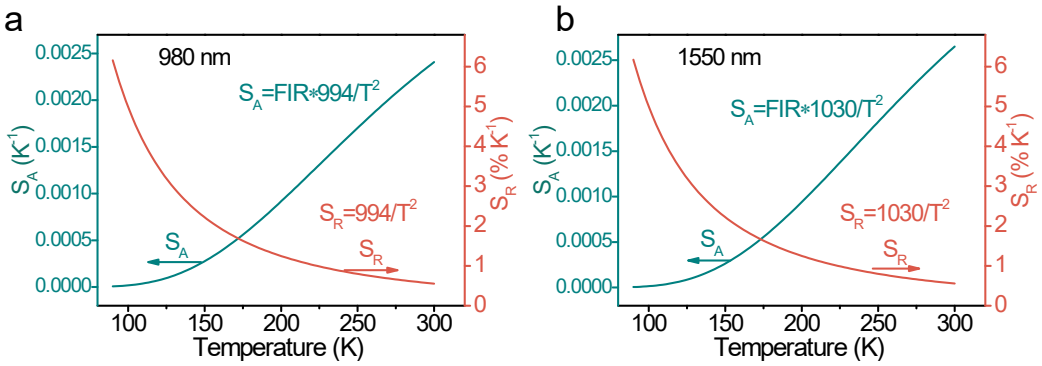

Figure S10. Absolute and relative sensitivities of temperature sensing based on TCL of $^2H_{11/2}/^4S_{3/2}$ under (a) 980 nm and (b) 1550 nm laser excitation.

The temperature sensitivity of TCL (G1/G2) are calculated, where the absolute sensitivity (S_A) keep increasing, while the relative sensitivity (S_R) keep decreasing in the experimental temperature range under whether 980 nm or 1550 nm laser excitation. The maximal value of S_A is obtained to be 0.0024 K^{-1} at 300 K, while the maximal value of S_R is obtained to be 6.1 $\%K^{-1}$ at 90 K under 980 nm excitation. The maximal value of S_A is obtained to be 0.0026 K^{-1} at 300 K, while the maximal value of S_R is obtained to be 6.2 $\%K^{-1}$ at 90 K under 1550 nm excitation. The results indicate that the maximum S_A and S_R of GC material are identical under different wavelength (980 or 1550 nm) laser excitation.

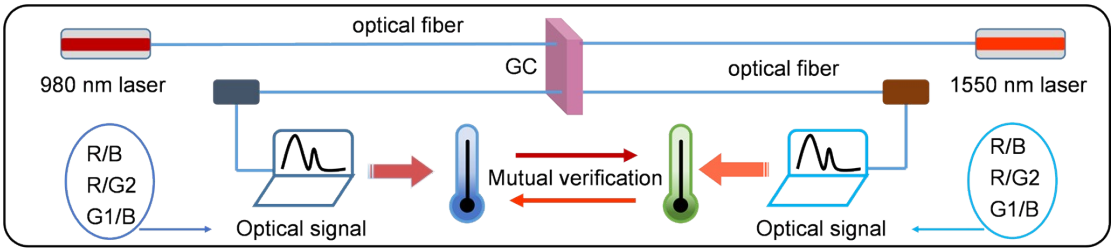

Figure S11. Schematic diagram of dual-mode optical temperature sensing based on GC material.

The GC material could be used to design a dual-mode temperature sensing, where the 980 and 1550 nm laser source excite the GC sensing device through a commercial fiber, and generated UC emission signal is further collected and passed back to spectra detection equipment by fiber. The two sets of temperature-related FIR information generated under the excitation of two excitation sources (980 and 1550 nm) can realize the mutual verification and self-calibration of optical temperature measurement, which could further ensure the accuracy and reliability of the detection.

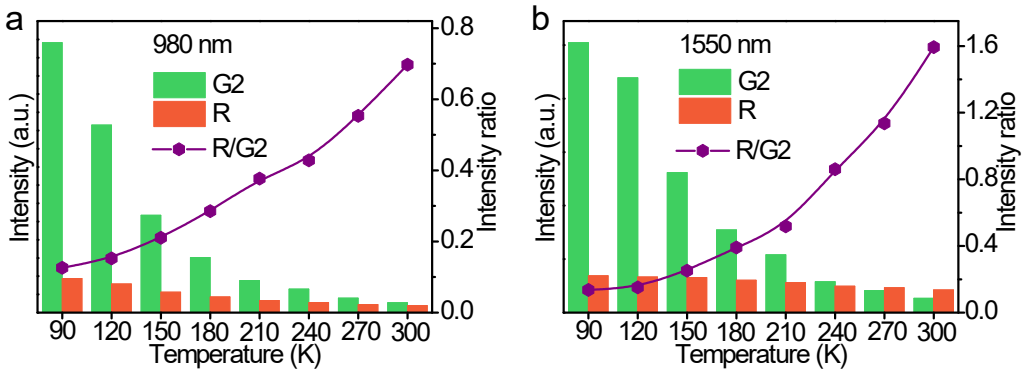

Figure S12. The integrated UC intensities of G2 and R emission and the emission intensity ratio under (a) 980 nm and (b) 1550 nm laser excitation at various temperatures.

As the temperature increase from 90 K to 300 K, the luminescence intensities of G2 and R emission both decrease under different excitation conditions (980 or 1550 nm laser), while the G2 emission intensity decreases more significantly. The R/G2 emission ratio both have increasing tendency under 980 or 1550 nm excitation, which could be used for optical thermometry based on FIR technique.

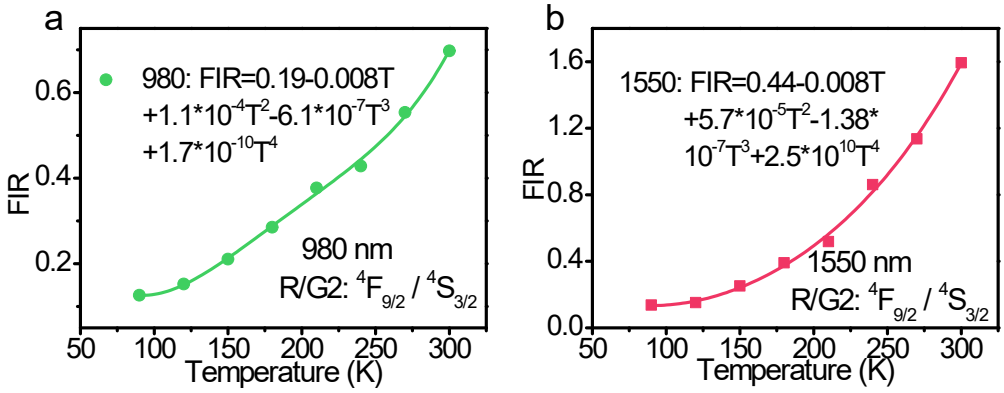

Figure S13. Temperature dependence of FIR based on NTCL of $^4F_{9/2}/^4S_{3/2}$ under (a) 980 and (b) 1550 nm excitation.

Since the expression for thermally coupled levels is not appropriate for NTCL, the experimental value of FIR in case of the NTCL could be fitted with simple polynomial equation. For the NTCL of $^4F_{9/2}$ and $^4S_{3/2}$, the value of the FIR can be obtained from the emission ratio R/G2. Under 980 nm or 1550 nm excitation, the FIR both increase with temperature and the experimental data could be well fitted by polynomial function.

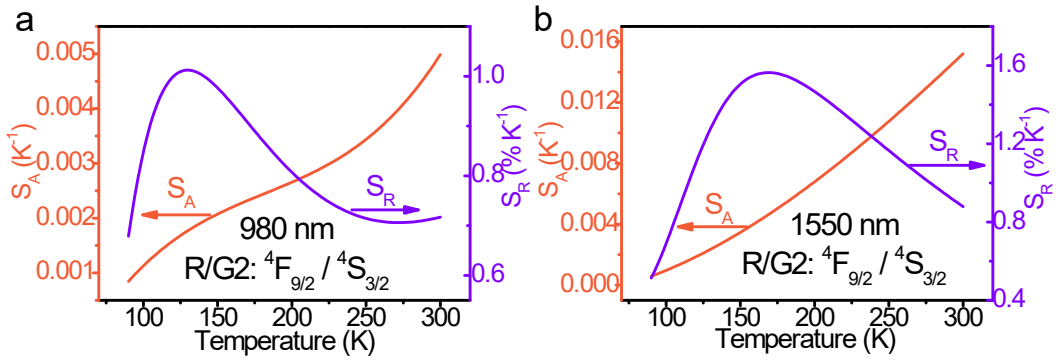

Figure S14. Absolute and relative sensitivities of temperature sensing based on NTCL of $^4F_{9/2}/^4S_{3/2}$ under (a) 980 nm and (b) 1550 nm laser excitation.

The temperature sensitivities for R/G2 (S_A and S_R) are calculated under whether 980 or 1550 nm excitation, where S_A continue to increase and S_R first increase and then decrease with increasing the temperature. The maximal value of S_A is obtained to be 0.005 K^{-1} at 300 K, while the maximal value of S_R is obtained to be 1.102 $\%K^{-1}$ at 130 K under 980 nm excitation. The maximal value of S_A is obtained to be 0.015 K^{-1} at 300 K, while the maximal value of S_R is obtained to be 1.564 $\%K^{-1}$ at 170 K under 1550 nm excitation.

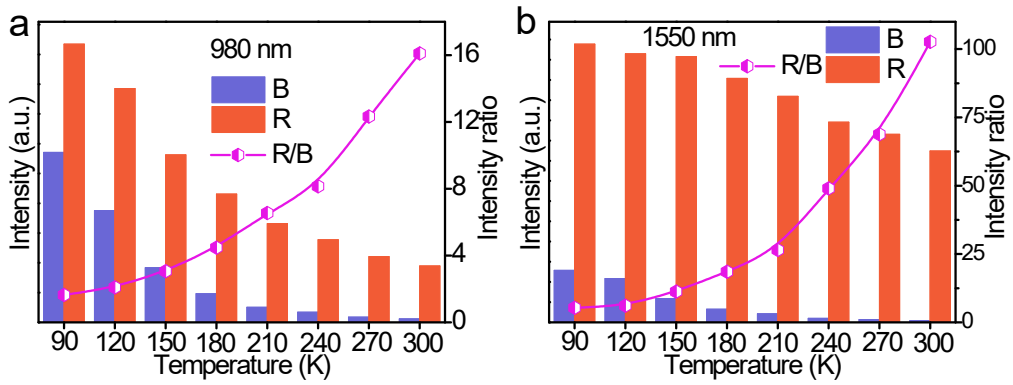

Figure S15. The integrated UC intensities of B and R emission and the emission intensity ratio under (a) 980 nm and (b) 1550 nm laser excitation at various temperatures.

As the temperature increase from 90 K to 300 K, the luminescence intensities of B and R emission both decrease under different excitation conditions (980 or 1550 nm laser), while the B emission intensity decreases more significantly. The R/B emission ratio both have increasing tendency under 980 or 1550 nm excitation, which could be used for optical thermometry based on FIR technique.

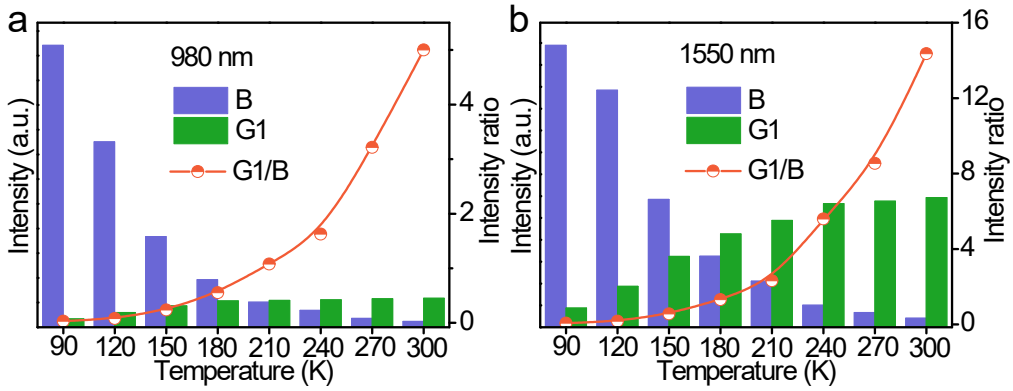

Figure S16. The integrated UC intensities of B and G1 emission and the emission intensity ratio under (a) 980 nm and (b) 1550 nm laser excitation at various temperatures.

As the temperature increase from 90 K to 300 K, the luminescence intensity of B emission decrease while G1 emission increase under different excitation conditions (980 or 1550 nm laser). The G1/B emission ratio both have increasing tendency under 980 or 1550 nm excitation, which could be used for optical thermometry based on FIR technique. Moreover, the B and G1 emissions exhibit the more remarkable change, which could provide the higher temperature sensing sensitivity.

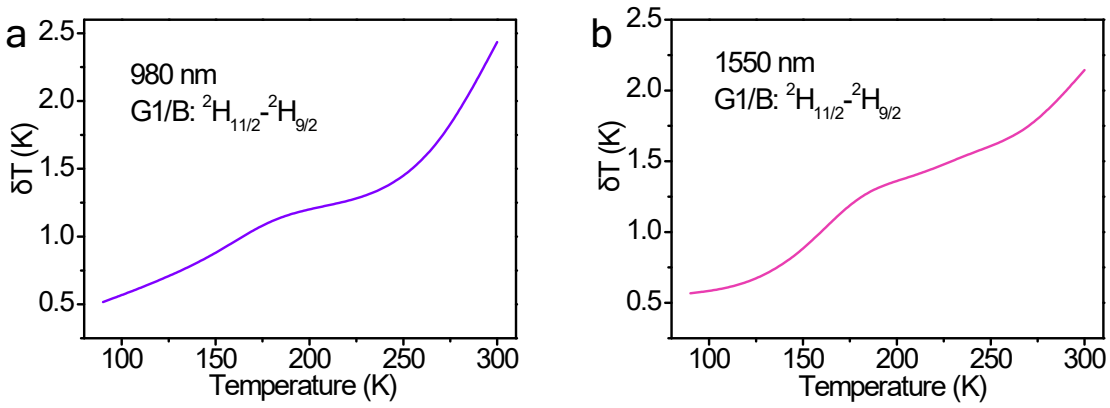

Figure S17. Temperature resolution of Er,Yb:$NaYF_4$ GC material based on $^2H_{11/2}$/$^2H_{9/2}$ NTCL under (a) 980 nm and (b) 1550 nm excitation

The temperature uncertainty (δT), also known as the temperature resolution or thermal resolution (ΔT), is another important parameter in optical temperature sensing, which represents the smallest detectable temperature change. The temperature uncertainty δT or temperature resolution ΔT can be described by the following equation:

$$\delta T = \Delta T = \frac{1}{S_R}\frac{\delta FIR}{FIR} \#(1)$$

where the δFIR/FIR is the uncertainty on the calculation of FIR, which is mainly related to the measuring devices and testing conditions. And δFIR/FIR can be written as:

$$\frac{\delta FIR}{FIR} = \sqrt{\left(\frac{\delta I_1}{I_1}\right)^2 + \left(\frac{\delta I_2}{I_2}\right)^2} \#(2)$$

where $\delta I_1/I_1$ and $\delta I_2/I_2$ are the intensity uncertainties of the corresponding emissions. The δI is the uncertainty by the readout fluctuations of the baseline, and I is the average intensity

evaluated over the whole emission spectral range. The average intensity I in the whole emission spectra range (E_0<E<E_1) is given by:[1,2]

$$I = \frac{\int_{E_0}^{E_1} I(E)\, dE}{E_1 - E_0} \#(3)$$

Finally, the quantification of the temperature uncertainty δT is achieved based on the above formulas.

The temperature resolution based on $^2H_{11/2}$-$^2H_{9/2}$ NTCL (G1/B) temperature measurement was analyzed, which could be used to further evaluate the potential of temperature sensor. We calculated the $\delta I_1/I_1$ and $\delta I_2/I_2$ values through dividing the readout fluctuations of the baseline by the average emission intensity value of 530 nm (G1) and 409 nm (B), respectively. The averaged δFIR/FIR value is about 3% under 980 nm excitation, and is about 2.9% under 1550 nm excitation. Finally, the temperature resolution δT of Er,Yb:$NaYF_4$ GC material were calculated with the Equation 1 under 980 nm and 1550 nm excitation. As shown in Fig. S17, the thermal resolution value are all below 2.5 K throughout the detected range of 90 K-300 K under excitation at 980 nm and 1550 nm. At 90 K, the GC material has the minimum temperature resolution values of 0.51 K (980 nm) and 0.56 K (1550 nm), which indicates its excellent ability to distinguish small temperature changes at low temperature and ensure the sufficient reliability.

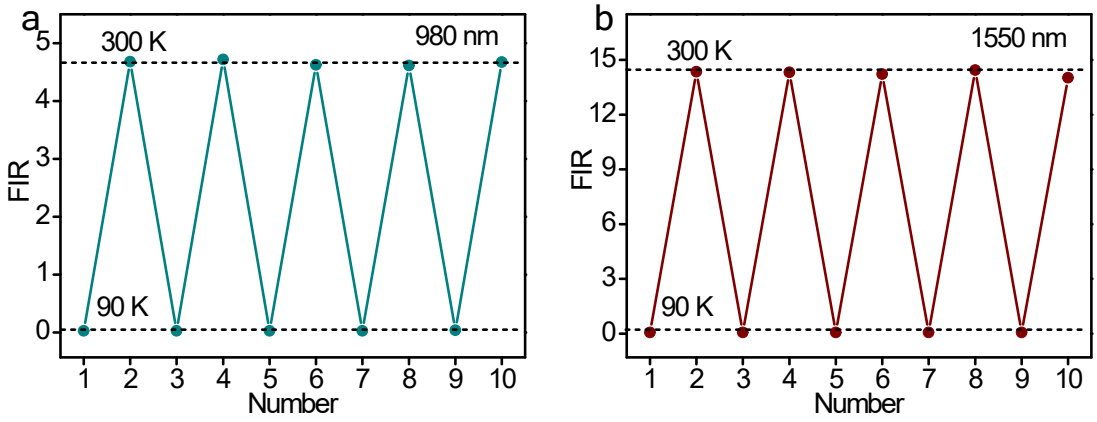

Figure S18. The temperature-recycle measurements of FIR values of Er,Yb:$NaYF_4$ GC material based on $^2H_{11/2}$-$^2H_{9/2}$ NTCL under (a) 980 nm and (b) 1550 nm excitation.

The repeatability of GC temperature sensor readings is also a key property, estimated by cycling over a given temperature interval

$$R = 1 - \frac{max(|FIR_C - FIR_i|)}{FIR_C} \#(4)$$

where FIR_C is the mean thermometric signal from different cycles and FIR_i is the thermometric signal in each cycle. The repeatability of the measurements of the GC material were evaluated by means of five consecutive heating-cooling cycles in the 90 K-300 K range. The calculated repeatability of proposed GC sensor based on $^2H_{11/2}$-$^2H_{9/2}$ NTCL were 98.7% and 98.2% under 980 nm and 1550 nm excitation, respectively.

Table S1. Color coordinates of the GC sample at different temperature under 980 nm laser excitation.

Temperature(K)	x	y
90	0.2919	0.685
120	0.2919	0.6858
150	0.2937	0.6835
180	0.2961	0.6808
210	0.2985	0.6774
240	0.2997	0.676
270	0.3013	0.6716
300	0.3026	0.667

Table S2. Color coordinates of the GC sample at different temperature under 1550 nm laser excitation.

Temperature(K)	x	y
90	0.2892	0.6966
120	0.289	0.6966
150	0.2935	0.6914
180	0.2997	0.6845
210	0.3075	0.6754
240	0.318	0.6627
270	0.3286	0.6473
300	0.3367	0.6406

References

1. M. Back, E. Trave, J. Ueda and S. Tanabe, *Chem. Mater.*, 2016, **28**, 8347-8356.
2. M. Back, E. Casagrande, E. Trave, D. Cristofori, E. Ambrosi, F. Dallo, M. Roman, J. Ueda, J. Xu, S. Tanabe, A. Benedetti and P. Riello, *ACS Appl. Mater. Interfaces*, 2020, **12**, 55195-55204.